Chinese Chemical Letters 34 (2023) 108439

Contents lists available at ScienceDirect

Chinese Chemical Letters

journal homepage: www.elsevier.com/locate/cclet

9,10-Bis(diphenylmethylene)-9,10-dihydroanthracene-based metal-organic assemblies with aggregation-induced emission for multiple sensing☆

Qian Feng[a,b], Nan Li[c], Zeyuan Zhang[a], Kai Gao[a], Kai Wang[c], Sanliang Ling[d], Hongye Yuan[a,*], Yanmin Zhang[b,*], Mingming Zhang[a,*]

[a] State Key Laboratory for Mechanical Behavior of Materials, Shaanxi International Research Center for Soft Matter, School of Materials Science and Engineering, Xi'an Jiaotong University, Xi'an 710049, China
[b] School of Pharmacy, Health Science Center, Xi'an Jiaotong University, Xi'an 710061, China
[c] State Key Laboratory of Superhard Materials, College of Physics, Jilin University, Changchun 130012, China
[d] Advanced Materials Research Group, Faculty of Engineering, University of Nottingham, Nottingham NG7 2RD, United Kingdom

ARTICLE INFO

Article history:
Received 21 February 2023
Revised 30 March 2023
Accepted 7 April 2023
Available online 7 April 2023

Keywords:
Light-emitting materials
Butterfly-like assembles
Aggregation-induced emission
Multiple sensing

ABSTRACT

Developing novel emissive supramolecular assemblies with elegant architectures and tunable performance remains highly desirable yet challenging. Herein, we report the design and synthesis of several 9,10-bis(diphenylmethylene)-9,10-dihydroanthracene-based metal-organic assembles with aggregation-induced emission characteristics. Such assemblies feature intriguing thermochromic and mechanochromic properties, *i.e.*, distinguishable fluorescence responses in terms of emission wavelength and intensity under variable temperatures and pressures. Moreover, these assemblies can serve as excellent fluorescent sensors for the detection of polysaccharide molecules. Due to the differentiated charge type and density, the assembles display distinct sensing mechanisms toward different polysaccharide molecules. This study provides novel perspectives for the synthesis of butterfly-like platinum(II) supramolecular coordination complexes with multistimuli-responsiveness for polysaccharide sensing, which will facilitate the development of stimuli-responsive materials

Light-emitting materials have received wide-ranging attention owing to their broad application such as chemical and biological sensors [1–8], bio-imaging agents [9–15], optoelectronic devices [16–18]. However, conventional fluorophores usually show aggregation-caused quenching (ACQ) properties [19–23], which is unfavorable for bio-applications because the hydrophobic fluorophores are easily to aggregate in aqueous environments. Fluorophores with aggregation-induced emission (AIE) properties, which are weakly emissive in dissolved state and highly emissive in aggregated state, serve as alternative candidates for bio-applications [24]. The AIE fluorophores feature high signal to noise ratio, good stability, fast response, high sensitivity, and fine linear concentration dependence [25–27], meeting the requirements as ideal candidates for sensing. Moreover, the twisted aromatic rings of AIE molecules are more sensitive to external stimuli (pressure, temperature and/or light), offering them switchable luminescence [28,29]. Due to their excellent emission and diverse stimuli-responsive performance, intensive investigations are expected for the preparation of multiple-sensing materials [30,31].

Coordination-driven self-assembly provides a facile and efficient method to construct various supramolecular coordination complexes (SCCs) with elegant structures and appealing physicochemical properties [32–46]. Incorporation of AIE fluorophores into SCCs affords diverse geometries and cavities for hosting specific biomolecules, tunable optical properties as well as integration of extra functions [28,47-53]. For example, Stang and co-workers prepared a series of emissive SCCs by introducing tetraphenylethylene (TPE) groups within the SCCs and realized their application in sensing, bio-imaging and light-emitting devices [5,10,54,55]. Although great progress has been made on the design and synthesis of AIE-based SCCs, their underlining structure-property needs to be well elucidated, of course, demanding more efforts. Furthermore, multi-stimuli responsive luminescent materials based on SCCs are still in the infancy, so their applications in biosensors and smart luminescent materials are still ambiguous.

☆ This paper is dedicated to the memory of Prof. Jiang Wei.

* Corresponding authors.
E-mail addresses: hongye.yuan@xjtu.edu.cn (H. Yuan), zhang2008@xjtu.edu.cn (Y. Zhang), mingming.zhang@xjtu.edu.cn (M. Zhang).

https://doi.org/10.1016/j.cclet.2023.108439
1001-8417/

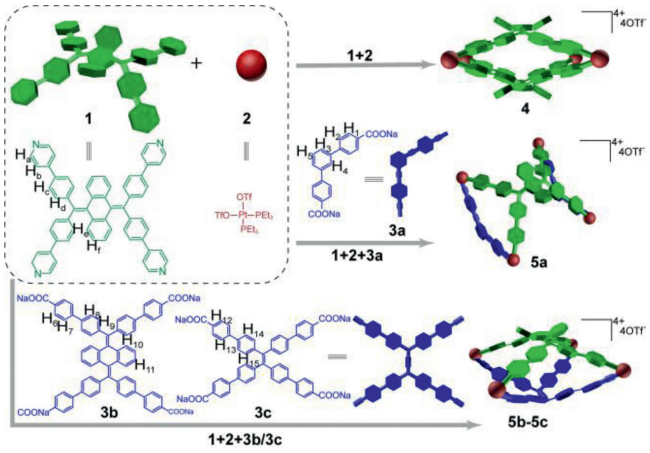

Scheme 1. Graphical illustrations for self-assembly of assemblies **4**, **5a-5c**.

9,10-Bis(diphenylmethylene)−9,10-dihydroanthracene (BDPM-DHA) and its derivatives [56,57] possess not only a graceful butterfly-like structure but also attractive optical feature, promising for multi-stimuli-responsive light-emitting materials. Herein, we report four BDPM-DHA-based metal-organic assemblies (**4**, **5a-5c**) *via* coordination-driven self-assembly (Scheme 1). Apart from **5c**, the fluorescence of these assemblies increases dramatically by increasing the proportion of water, suggesting their AIE nature. Additionally, these assemblies exhibited tunable fluorescence behaviors with reduced emission intensity and red-shifted wavelength under increased temperatures and pressures. Upon the addition of negatively charged polysaccharide substances, the fluorescence of these positively charged assemblies (**4**, **5a** and **5b**) in solutions enhanced significantly owing to the formation of aggregations. This work presents the preparation of SCCs as sensitive sensors for diverse responses (temperature, pressure, polysaccharide), which paves the avenue for the development of emissive materials for multiple sensing applications.

The assemblies **4** and **5a-5c** were prepared (see Supporting information for synthetic details) and characterized by $^{31}P\{^{1}H\}$, ^{1}H NMR analysis as well as electrospray ionization time-of-flight mass spectrometry (ESI-TOF-MS). The $^{31}P\{^{1}H\}$ NMR spectrum of **4** displayed a sharp singlet (*ca.* −0.40 ppm) accompanied by two ^{195}Pt satellites (Fig. 1a). Two doublet peaks (*ca.* 5.38 and 0.00 ppm for **5a**, 5.08 ppm and 0.07 ppm for **5b**, 5.45 ppm and 0.09 ppm for **5c**) of approximately equal intensity were observed in Figs. 1b-d, demonstrating the distinct phosphorus environment of **5a-5c**, which were contributed by the coordination of N and O atoms on pyridyl and carboxylate moieties to Pt(II) center, respectively. As shown in Figs. 1e-i, the protons of **1**, **4** and **5a-5c** in ^{1}H NMR spectra was clearly identified. Compared with the ligand **1**, α-pyridyl proton (H_a) and β-pyridyl proton (H_b) of **4** split into two sets of peaks because of the protons located inside and outside of the assembly, while those of **5a-5c** showed significant downfield chemical shifts due to the coordination bonds. ESI-TOF-MS data further confirmed the chemical compositions of the assemblies (Figs. 1j-m). There were groups of peaks (3+ to 6+ for **4**, 2+ to 3+ for **5a**, 2+ to 4+ for **5b-5c**) corresponding to multi-charged species with the loss of OTf^- counterions. For instance, isotopically resolved peaks with *m/z* 761.1790 [**4**–5OTf]$^{5+}$, 1107.8278 [**5a**-3OTf]$^{3+}$, 1225.1946 [**5b**-3OTf]$^{3+}$ and 1166.5105 [**5c**-3OTf]$^{3+}$ were observed, whose assignments agreed well with their simulated isotopic distributions. These results jointly confirmed the successful formation of discrete supramolecular assembles [15,58-60].

Single crystals suitable for X-ray crystallographic analysis (Figs. 2a-c) of ligand **1** (CCDC: 2226633) and assemblies **4** (CCDC: 2226634) and **5a** (CCDC: 2226635) were successfully obtained by

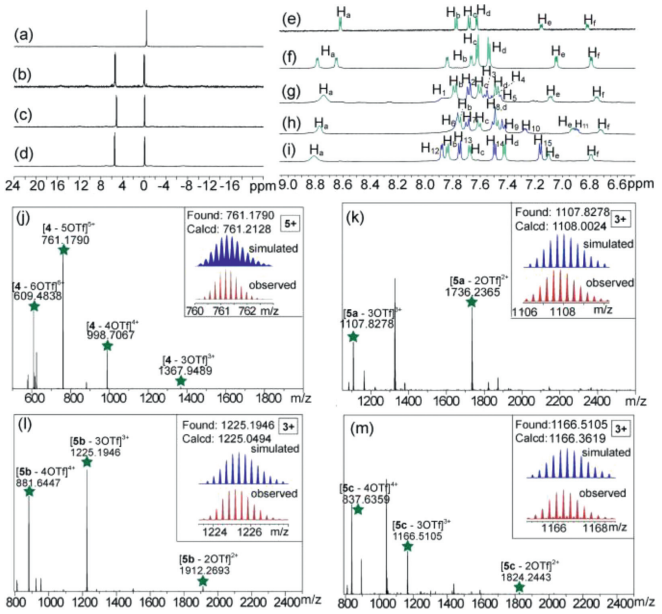

Fig. 1. Partial $^{31}P\{^{1}H\}$ NMR spectra (162 or 243 MHz, CD_3CN, 295 K) of (a) **4**, (b) **5a**, (c) **5b** and (d) **5c**. Partial ^{1}H NMR spectra (400 or 600 MHz, CD_3CN, 295 K) of (e) **1**, (f) **4**, (g) **5a**, (h) **5b** and (i) **5c**. ESI-TOF-MS spectra of (j) **4**, (k) **5a**, (l) **5b** and (m) **5c**.

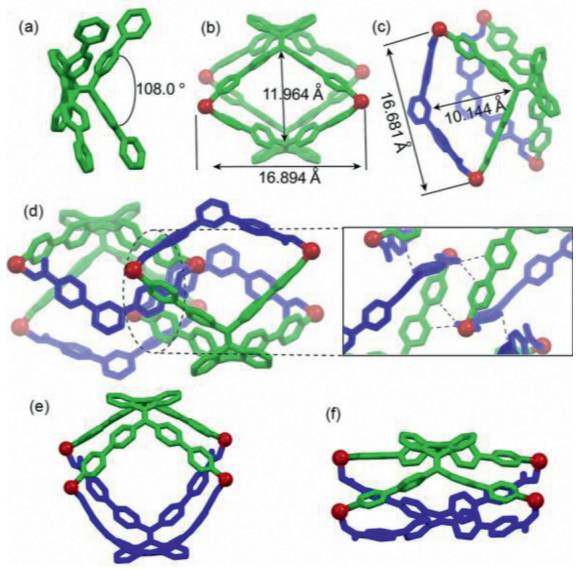

Fig. 2. Crystal structures of (a) **1**, (b) **4** and (c) **5a**. (d) Crystal packing of **5a**. Optimized molecular structures of (e) **5b** and (f) **5c** by DFT calculations. Hydrogen atoms, counterions, solvent molecules and triethylphosphine units are omitted for clarity.

slow vapor diffusion for 2 weeks at 4 °C (acetonitrile/isopropyl ether for **1**, **4** and acetonitrile/dioxane for **5a**). From the side view, two adjacent arms of ligand **1** bend with dihedral angles of 108.0°. The structure seems distorted conformationally, resembling like a butterfly, because of the obvious steric hindrance effect (Fig. 2a and Fig. S19 in Supporting information). Therefore, ligand **1** and the Pt ligand **2** are coordinated adaptively to form [2 + 4] modes during self-assembly. The two-component assembly **4** exhibits highly symmetrical geometry with a large diagonal cavity of 16.89 × 11.96 $Å^2$ (Fig. 2b), which is neatly arranged in the crystalline state to form a three-dimensional network structure (Fig. S20 in Supporting information). 3D double ring **5a** holds a butterfly structure with two open windows (the diagonal cavity: 16.68 × 10.14 $Å^2$).

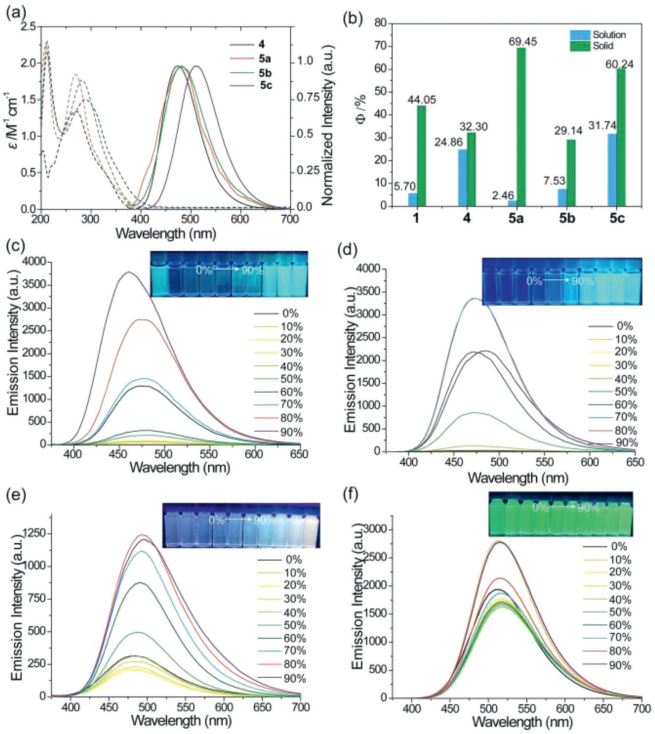

Fig. 3. (a) UV–vis absorption and normalized emission spectra of **4**, **5a**–**5c** in acetonitrile. (b) Absolute fluorescence quantum yields of **1**, **4**, **5a**-**5c** in acetonitrile and solid state. Emission spectra of (c) **4**, (d) **5a**, (e) **5b**, and (f) **5c** in mixed solutions of acetonitrile and water in different volume ratios. Insets: photographs of **4**, **5a**–**5c** in different fractions of mixed solutions ($\lambda_{ex} = 365$ nm, $c = 10.0$ μmol/L).

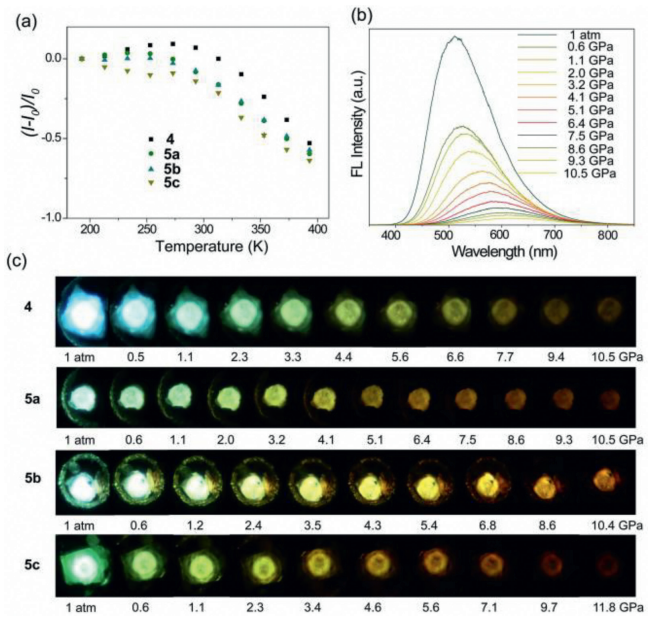

Fig. 4. (a) $(I\text{-}I_0)/I_0$ of **4**, **5a-5c** at various temperatures in solid state. (b) Emission spectra of **5a** and (c) fluorescent images of **4**, **5a-5c** under external pressures.

Interestingly, a unit cell contains two molecules that interact with each other to form a partially crossed structure (Fig. 2d and Fig. S21 in Supporting information). The attempts to obtain the crystal structures of assemblies **5b** and **5c** failed. Therefore, density functional theory (DFT) calculations were carried out to deeply understand the structures. Based on the mass data, both **5b** and **5c** were assembled by **1**, **2**, and **3b**/**3c** in 1:4:1 molar ratio, forming a similar structure like **5a**. The DFT calculated structures indicated that the carboxylate ligands in **5b**/**5c** were highly twisted. The cavity of **5b** was larger than that of **4**, and the cavity of **5c** was smaller than that of **4**. These results suggested that the cavity size of the supramolecular assemblies could be finely tuned by the addition of carboxylate ligands as building blocks, showing the advantages of multicomponent coordination-driven self-assembly. However, owing to the twist aromatic groups in such assemblies, no good host-guest chemistry was observed for these metallacages.

The UV–vis absorption and fluorescence spectra of the assemblies were collected to investigate their photophysical behaviors. These assemblies were well-dissolved in CH_3CN. Their absorption was in the region of 200 nm to 400 nm. From fluorescence spectra, peaks centered at 479 nm, 483 nm, 484 nm and 511 nm were observed (Fig. 3a), corresponding to **4** and **5a**-**5c**, respectively. It could be found that the emission of **4**, **5a** and **5b** is mainly derived from the characteristic emission of BDPM-DHA and the emission of **5c** was mainly contributed by the TPE units. The fluorescence quantum yields (Φ_F) of **1**, **4** and **5a**-**5c** were measured to be 5.7%, 24.86%, 2.46%, 7.53%, and 31.74%, respectively, in acetonitrile (Fig. 3b and Figs. S23-S32 in Supporting information). The assembly **5a** displayed the highest emission intensity in solid state (Φ_F = 69.45%). Therefore, **5a** was considered to be a good candidate for chemical/biosensing owing to its larger fluorescence difference upon external stimuli. The AIE characteristics of these assemblies were investigated by recording the fluorescence emission with increasing water content in the mixed solvent (acetonitrile/water) (Figs. 3c-f and Fig. S33 in Supporting information). The fluorescence intensity of **4** increased significantly once the water content was over 60%, showing typical AIE characteristics. A similar phenomenon also appeared for **5a** and **5b**, although the fluorescence of the two complexes was weak in acetonitrile. When the water fraction increased to 90%, the fluorescence intensity decreased slightly due to the enhanced intermolecular collisions of the assembly **5a**-**5b** [53,61]. Interestingly, the maximum emission of **5b** was significantly red-shifted, and the color gradually changed from light blue to light yellow. However, the AIE characteristic of **5c** was unobvious, because the addition of water can't improve the fluorescence dramatically.

In order to further explore the effect of external stimuli on the luminescent properties and their potential use for stimuli-responsive light-emitting materials, the fluorescence spectra of assemblies in liquid and solid state at distinct temperatures were recorded (Fig. 4a and Figs. S34-S41 in Supporting information). The emission intensity changed slightly before 273 K, while it decreased almost linearly with the increment of temperature in the solid state. In acetonitrile, as the temperature rose from −20°C to 60 °C, the intensity of these assemblies weakened gradually linearly, while the maximum emission wavelength hardly changed. The decrease of emission intensity is because that molecular motions are enhanced to dissipate the energy of the molecular excited state as the increase of temperature [62]. Accordingly, these assemblies can be employed for fluorescent thermometers based on AIE effects to sensitively detect temperature variation.

Mechanochromic materials represent a class of smart light-emitting materials, which respond to external force stimuli [63,64]. To explore the influence of pressure on the emission in solid state, the fluorescence spectra and images under variable pressures were collected using diamond anvil cell (DAC) technology. The photophysical behaviors of these assemblies witnessed a dramatic bathochromic shift both for absorption and emission, as well as decreases of emission intensity upon pressurization (Figs. 4b and c, Figs. S42 and S43 in Supporting information). For example, the maximum absorption of **5a** shifted from 393 nm to 460 nm, and its maximum emission shifted from 511 nm to 614 nm. The

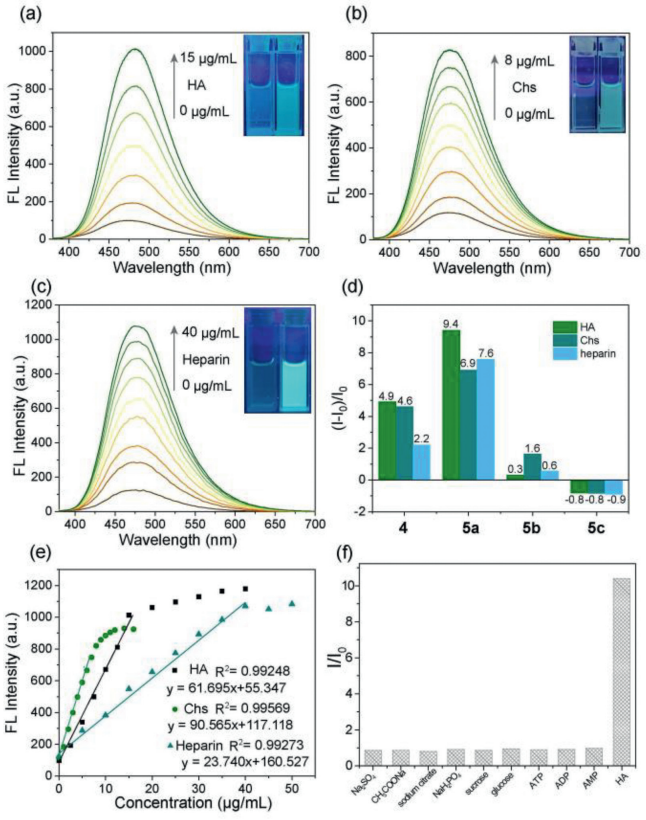

Fig. 5. Fluorescence spectra of **5a** at varied amount of (a) HA, (b) Chs and (c) heparin. (d) $(I\text{-}I_0)/I_0$ of **4**, **5a**-**5c** for HA, Chs and heparin. (e) The plots of fluorescence intensity of **5a** in the prescence of different concentrations of analytes. (f) Fluorescence responses of **5a** upon the addition of 10 equiv. of interfering analytes. ($\lambda_{ex} = 365$ nm, $c = 10$ μmol/L, acetonitrile/water = 1/1, v/v).

fluorescent color gradually changed from blue to orange under the pressure of 10.5 GPa. The mechanochromism likely originates from the planarization of structures under the external pressure, which would also lead to the closer arrangement of molecules [28,30]. As a consequence, the butterfly wings and the cavities were flattened, affecting the π-π stacking and dipole-dipole interactions, thus influencing the fluorescence emission. Moreover, the fluorescence quenching efficiency of various assemblies was different, and **5b** denotes the slowest one. Even upon the pressure of 10.4 GPa, a strong fluorescence could be observed. When the pressure was gradually released, the fluorescence continuously recovered (Figs. S44-S47 in Supporting information), and the emission was blue-shifted to the original wavelength, which further evidenced the responsive mechanochromism properties of these assemblies.

Given the existence of positive charges within these assemblies, we speculate that the addition of negatively charged biopolymers would induce emission changes, making them applied for biosensing. Therefore, we selected the sodium salts of hyaluronic acid (HA), chondroitin 4-sulfate (Chs) and heparin, which are negative polysaccharide polymers with different charge densities, as the candidates for sensing study. Fluorescence titration experiments were carried out by the addition of the three polysaccharides to assemblies **4**, **5a**-**5c** (Figs. 5a-c, and Figs. S48-S50 in Supporting information). Fluorescence intensity of **4**, **5a** and **5b** increased gradually with the addition of polysaccharides, and the maximum emission wavelength remained nearly invariant. However, the intensity of **5c** experienced a downward trend, and the wavelength was blue-shifted. To compare the sensitivity of these assemblies toward the three polysaccharides, their increased emission $(I\text{-}I_0)/I_0$ was plotted *versus* the concentration of analytes (Fig. 5d). The results implied that the fluorescence enhancement of **5a** was the highest one (9.4, 6.9 and 7.6-fold, respectively), indicating a better sensitivity and signal-to-noise ratio. We hereafter utilized the assembly **5a** to probe polysaccharides. The fitting linear ranges were 0–15, 0–8, 0–40 μg/mL, and the detection limit ($\text{LOD} = 3\sigma/S$) were calculated to be 0.73, 0.49 and 1.89 μg/mL for HA, Chs, heparin, respectively (Fig. 5e). To evaluate the selectivity of **5a** towards polysaccharide, various potential interfering substances were added into the solution of **5a** (Fig. 5f), including small molecular sodium salts (sodium sulfate, sodium acetate, sodium citrate, sodium dihydrogen phosphate), sugars (sucrose, glucose) and biological molecules (ATP, ADP, AMP). Only in the presence of polysaccharide, a significant increasement in fluorescence intensity was observed, which illustrated the high selectivity of **5a** for polysaccharides.

To better understand the interplay between **5a** and polysaccharides and to reveal the sensing mechanism, the morphology of **5a** with polysaccharides was studied by scanning electron microscopy (SEM). Irregular aggregates were found, which were formed by the electrostatic interactions between the negatively charged polysaccharides and positively charged **5a** (Fig. S51 in Supporting information), indicating that the addition of polysaccharides would force the aggregation of **5a**, inducing the increase of the emission. Furthermore, the addition of polysaccharide to **5a** were studied by $^{31}P\{^1H\}$ and ^1H NMR spectroscopy. The proton and phosphorus NMR spectra remained almost unchanged after the addition of HA and Chs, indicating that the structure of **5a** remained intact and not dissociated (Figs. S52 and S53 in Supporting information). However, as the addition of heparin to the deuterated solution of **5a**, the phosphorus signal showed an apparent downfield shift and two new doublet peaks appeared. Additionally, the proton signals also underwent significant changes, such as pyridyl proton (H_a) shifted upfield by 0.16 ppm. These findings prompted us to consider the possibility of a new assembly. To validate this point, ligands **1**, **2** (1:2 in molar ratio) and excessive heparin were self-assembled and their $^{31}P\{^1H\}$ and ^1H spectra were obtained (Fig. S54 in Supporting information). Two new doublet peaks were observed in the $^{31}P\{^1H\}$ spectra, and distinct proton signals were found in the ^1H NMR spectra. This result indicated that a new complex was formed between **1**, **2** and heparin, which is probably because of the formation of new metal-coordination bonds by the pyridyl groups of **1**, platinum ligand **2** and the carboxylate groups of heparins. Such complexation would also force the aggregation of **1**, giving increased emission upon the addition of heparin, which has also been observed in other metal-coordination complexes [5]. Therefore, for all the assemblies, the addition of polysaccharide would force the aggregation of fluorophores in the assemblies, offering increase emission for sensing.

In conclusion, a series of 9,10-bis(diphenylmethylene)–9,10-dihydroanthracene-based assemblies with butterfly-like structures were constructed, which exhibited obvious AIE characteristics. They also show tunable fluorescence behaviors under different temperatures and applied pressures. In addition, they exhibited obvious fluorescence responses to negatively charged polysaccharides. Such properties suggest these assemblies can serve as good candidates for multiple sensing. This work not only presents the design and synthesis of novel butterfly-like emissive assemblies, but also further explores their applications as fluorescent sensors toward temperature, pressure and biomolecules.

Declaration of competing interest

The authors declare that they have no known competing financial interests or personal relationships that could have appeared to influence the work reported in this paper.

Acknowledgments

This work was supported by the National Natural Science Foundation of China (Nos. 22171219 and 22222112), Innovation Talent Promotion Plan of Shaanxi Province for Science and Technology Innovation Team (2023-CX-TD-51), and the Fundamental Research Funds for the Central Universities. The authors thank Dr. Gang Chang and Dan He at the Instrument Analysis Center and Dr. Aqun Zheng and Junjie Zhang at the Experimental Chemistry Center of Xi'an Jiaotong University for NMR and fluorescence measurements. We thank Menghan Sun from Shiyanjia Lab (www.shiyanjia.com) for the X-ray crystal structure analysis. We also acknowledge the mass spectrometry characterization by the Molecular Scale Laboratory at Shenzhen University.

Supplementary materials

Supplementary material associated with this article can be found, in the online version, at doi:10.1016/j.cclet.2023.108439.

References

[1] L.Y. Niu, Y.Z. Chen, Q.Z. Yang, et al., Chem. Soc. Rev. 44 (2015) 6143–6160.
[2] J. Liang, B.Z. Tang, B. Liu, Chem. Soc. Rev. 44 (2015) 2798–2811.
[3] H.R. Xu, K. Li, X.Q. Yu, Chin. Chem. Lett. 26 (2015) 877–880.
[4] W.P. Lustig, S. Mukherjee, S.K. Ghosh, et al., Chem. Soc. Rev. 46 (2017) 3242–3285.
[5] M. Zhang, M.L. Saha, P.J. Stang, et al., J. Am. Chem. Soc. 139 (2017) 5067–5074.
[6] T.L. Mako, J.M. Racicot, M. Levine, Chem. Rev. 119 (2019) 322–477.
[7] H. Duan, F. Cao, L. Cao, et al., Chin. Chem. Lett. 33 (2022) 2459–2463.
[8] Y. Pan, Y. Guo, X. Yan, et al., Chin. Chem. Lett. 34 (2023) 108237.
[9] H.Q. Peng, L.Y. Niu, Q.Z. Yang, et al., Chem. Rev. 115 (2015) 7502–7542.
[10] M. Zhang, S. Li, P.J. Stang, et al., Proc. Natl. Acad. Sci. U. S. A. 113 (2016) 11100–11105.
[11] B. Wang, C. Nie, S. Wang, et al., Chin. Chem. Lett. 28 (2017) 1975–1978.
[12] S. Samanta, Y. He, J.S. Kim, et al., Chem 5 (2019) 1697–1726.
[13] H.B. Cheng, Y. Li, J. Yoon, et al., Chem. Soc. Rev. 49 (2020) 21–31.
[14] J. Dong, Y. Pan, D. Zhao, et al., Angew. Chem. Int. Ed. 59 (2020) 10151–10159.
[15] Q. Feng, T. Yang, L. Fan, et al., ACS Appl. Mater. Interfaces 14 (2022) 38594–38603.
[16] E. Cariati, E. Lucenti, S. Righetto, et al., Coord. Chem. Rev. 306 (2016) 566–614.
[17] B. Pashaei, S. Karimi, F. Bonaccorso, et al., Chem. Soc. Rev. 48 (2019) 5033–5139.
[18] C. Mu, Z. Zhang, M. Zhang, et al., Angew. Chem. Int. Ed. 60 (2021) 12293–12297.
[19] Y. Hong, J.W.Y. Lam, B.Z. Tang, Chem. Soc. Rev. 40 (2011) 5361–5388.
[20] J. Mei, N.L.C. Leung, B.Z. Tang, et al., Chem. Rev. 115 (2015) 11718–11940.
[21] M. Yamashina, M.M. Sartin, M. Yoshizawa, et al., J. Am. Chem. Soc. 137 (2015) 9266–9269.
[22] C. Qin, Y. Li, L. Cao, et al., Chin. Chem. Lett. 32 (2021) 3531–3534.
[23] S. Qin, H. Zou, L. You, et al., Chin. Chem. Lett. 33 (2022) 3267–3271.
[24] C. Zhou, W. Xu, B.Z. Tang, et al., Adv. Funct. Mater. 29 (2019) 1805986.
[25] R. Hu, N.L.C. Leung, B.Z. Tang, Chem. Soc. Rev. 43 (2014) 4494–4562.
[26] R.T.K. Kwok, C.W.T. Leung, B.Z. Tang, et al., Chem. Soc. Rev. 44 (2015) 4228–4238.
[27] X. Jiang, H. Gao, L. Jiang, et al., Nat. Commun. 9 (2018) 3799.
[28] Z. Zhang, Z. Zhao, M. Zhang, et al., J. Am. Chem. Soc. 142 (2020) 2592–2600.
[29] L.X. Cai, D.N. Yan, Q.F. Sun, J. Am. Chem. Soc. 143 (2021) 2016–2024.
[30] Y. Li, T. Yang, Y.F. Han, et al., CCS Chem. 4 (2022) 732–743.
[31] J. Zhang, H. Shen, B.Z. Tang, et al., Angew. Chem. Int. Ed. 61 (2022) e202208460.
[32] Y. Inokuma, M. Kawano, M. Fujita, Nat. Chem. 3 (2011) 349–358.
[33] T.R. Cook, P.J. Stang, Chem. Rev. 115 (2015) 7001–7045.
[34] C.J. Brown, F.D. Toste, K.N. Raymond, et al., Chem. Rev. 115 (2015) 3012–3035.
[35] B.M. Schmidt, T. Osuga, M. Fujita, et al., Angew. Chem. Int. Ed. 55 (2016) 1561–1564.
[36] W. Wang, Y.X. Wang, H.B. Yang, et al., Chem. Soc. Rev. 45 (2016) 2656–2693.
[37] G.H. Clever, P. Punt, Acc. Chem. Res. 50 (2017) 2233–2243.
[38] S. Chakraborty, G.R. Newkome, Chem. Soc. Rev. 47 (2018) 3991–4016.
[39] G.Y. Wu, L.J. Chen, H.B. Yang, et al., Coord. Chem. Rev. 369 (2018) 39–75.
[40] F.J. Rizzuto, L.K.S. von Krbek, J.R. Nitschke, Nat. Rev. Chem. 3 (2019) 204–222.
[41] R. Saha, A. Devaraj, P.S. Mukherjee, et al., J. Am. Chem. Soc. 141 (2019) 8638–8645.
[42] Y. Sun, C. Chen, P.J. Stang, et al., Chem. Soc. Rev. 49 (2020) 3889–3919.
[43] S. Bhattacharyya, S.R. Ali, P.S. Mukherjee, J. Am. Chem. Soc. 142 (2020) 18981–18989.
[44] P.C. Purba, M. Maity, P.S. Mukherjee, et al., Angew. Chem. Int. Ed. 60 (2021) 14109–14116.
[45] H. Liu, Z. Zhang, M. Zhang, et al., Angew. Chem. Int. Ed. 61 (2022) e202207289.
[46] Z. Zhang, L. Ma, M. Zhang, et al., JACS Au 2 (2022) 1479–1487.
[47] L.J. Chen, Y.Y. Ren, H.B. Yang, et al., J. Am. Chem. Soc. 137 (2015) 11725–11735.
[48] Y. Tian, X. Yan, P.J. Stang, et al., J. Am. Chem. Soc. 138 (2016) 12033–12036.
[49] X. Wang, Q. Su, M. Zhang, et al., Chem. Commun. 56 (2020) 8460–8463.
[50] Y. Hou, Z. Zhang, M. Zhang, et al., J. Am. Chem. Soc. 142 (2020) 18763–18768.
[51] Y.X. Hu, X. Hao, H.B. Yang, et al., J. Am. Chem. Soc. 142 (2020) 6285–6294.
[52] Y. Hou, Z. Zhang, M. Zhang, et al., CCS Chem. 4 (2022) 2604–2611.
[53] Z. Zhang, Y. Huang, P. Wang, et al., JACS Au 2 (2022) 2809–2820.
[54] X. Yan, T.R. Cook, P.J. Stang, et al., Nat. Chem. 7 (2015) 342–348.
[55] X. Yan, M. Wang, P.J. Stang, et al., J. Am. Chem. Soc. 138 (2016) 4580–4588.
[56] Z. He, L. Zhang, B.Z. Tang, et al., Chem. Mater. 27 (2015) 6601–6607.
[57] Z. He, L. Shan, B.Z. Tang, et al., Chem. Sci. 6 (2015) 3538–3543.
[58] L. Ma, T. Yang, M. Zhang, et al., Chin. Chem. Lett. 30 (2019) 1942–1946.
[59] Y. Hou, R. Shi, M. Zhang, et al., Chin. Chem. Lett. 34 (2022) 107688.
[60] K. Gao, Q. Feng, M. Zhang, et al., Angew. Chem. Int. Ed. 61 (2022) e202209958.
[61] Z. Chi, X. Zhang, J. Xu, et al., Chem. Soc. Rev. 41 (2012) 3878–3896.
[62] Y. Yang, S. Zhang, Y. Ji, et al., Nat. Commun. 10 (2019) 3165.
[63] Q. Qi, J. Qian, W. Tian, et al., Adv. Funct. Mater. 25 (2015) 4171-4171.
[64] T. Han, L. Liu, B.Z. Tang, et al., Macromol. Rapid. Commun. 42 (2021) e2000311.